Tailoring hydroxyapatite suspensions by stirred bead milling

Pedro Navarrete-Segado, Mallorie Tourbin, David Grossin, Christine Frances

Ceramics International 48 (2022) 24953–24964

Contents lists available at ScienceDirect

Ceramics International

journal homepage: www.elsevier.com/locate/ceramint

Tailoring hydroxyapatite suspensions by stirred bead milling

P. Navarrete-Segado [a,b], M. Tourbin [b], D. Grossin [a], C. Frances [b,*]

[a] CIRIMAT, Université de Toulouse, CNRS, 4 Allée Émile Monso, 31030, Toulouse Cedex 4, France
[b] Laboratoire de Génie Chimique, Université de Toulouse, CNRS, 4 Allée Émile Monso, 31432, Toulouse Cedex 4, France

A R T I C L E I N F O

Keywords:
Hydroxyapatite
Ceramic suspension
Powder technology
Additive manufacturing
Wet milling

A B S T R A C T

The present work deals with the use of stirred bead milling process to tune the hydroxyapatite particles size adjusting the process conditions. Our goal is to find the optimal parameters to obtain particulate suspensions within a 0.2–1.5 μm particle size range. This size range is preferable to produce spherical feedstock for powder bed fusion technologies through the atomization process. A Darvan C dispersant agent dosage of 2.1 mg m^{-2} (active component) to the specific surface of the ceramic was found, through stability and rheological analyses, to be the most outstanding dosage for stabilizing the dispersion. Milling chamber, bead wear, and energy consumption were evaluated and minimized, finding the most efficient operating parameter setting for the process. For the studied material, the use of a fast stirrer speed, smaller grinding media size, and higher solids concentration increased the energy efficiency. This work confirmed the presented laboratory-scale milling process as a promising method to study the processing of hydroxyapatite-filled slurries, as a first-step product, on the manufacture of hydroxyapatite microspheres for the powder bed fusion industry.

1. Introduction

Additive manufacturing (AM) technologies have demonstrated the feasibility of producing ceramic parts for tissue engineering and implantology through different categories, such as powder bed fusion (PBF) [1,2]. This group of techniques might produce convenient, fast, and individualized implants, shortening the production period of patient-matched tissue engineering scaffolds from a bio-ceramic powder feedstock, as hydroxyapatite (HA) [3,4]. HA is already a well-known calcium phosphate-based bio-ceramic material, frequently used in bone tissue engineering because of its suitable properties for bone tissue reparation [5]. Its bioactivity and biocompatibility ensure the osseointegration of the implants while keeping their mechanical properties [6].

At the time of tailoring the powder feedstock properties, it is necessary to know the needs for the technique in which it will be used. In the case of PBF techniques, a homogeneous powder bed is preferably achieved by flowable spherical particles with a median particle size, x_{50}, between 30 and 70 μm [4,7]. Various material studies [8–12] have shown how the larger size and spherical shape improve the flowability of powders. A Hausner ratio lower than 1.25 (which is known to be characteristic of high flowability) should be obtained for the powder, which is recommended for PBF powders [13]. Thus the production of an optimal PBF powder feedstock should involve a previous process step like spray-drying to shape the ceramic particles into spherical granules [14].

In a spray-drying process, it is known that the size of the primary particles present in the liquid suspension feedstock has an effect on the spray formation, morphology and internal structure of the produced granules. Several studies have demonstrated that higher heat transfer efficiency (resulting in the lowest moisture content of the granules) and more solid, spherical and dense granules are obtained when using ceramic primary particles having an x_{50} commonly in the range of 0.2–1.5 μm [15–18]. A high concentration of solutes in the liquid (thus reducing the volume of liquid to evaporate) is desirable to increase dryer thermal efficiency [19]. However, a higher solids concentration can lead to an increase of the slurry viscosity. If it is too high, it can cause the grinding media to be stuck on the surface of the grinding chamber affecting the comminution of the particles and the fineness of the obtained particles [20]. It could also bring handling difficulties during the spray-drying process itself, especially during the pumping and mixing of the slurry [21]. The successful spray-drying of ceramic slurries having viscosities up to 0.1 Pa s has been reported previously [15]. Thus, the tailoring of the particulate suspensions is preferred before its utilization as feedstock in a spray-drying process. The particle size reduction by stirred bead milling will be the focus of the present paper. The next steps (drying, agglomeration, and shaping from powder into solid parts) have been discussed in recent works [22,23].

* Corresponding author.
E-mail address: christine.frances@ensiacet.fr (C. Frances).

https://doi.org/10.1016/j.ceramint.2022.05.149
Received 20 January 2022; Received in revised form 28 April 2022; Accepted 13 May 2022
Available online 21 May 2022

Abbreviations

AM = Additive Manufacturing
BET = Brunauer–Emmett–Teller
DC = Darvan C
FTIR = Fourier Transform Infrared Spectroscopy
GM = Grinding Media
HA = Hydroxyapatite
ICP-AES = Inductively Coupled Plasma Atomic Emission Spectroscopy
PBF = Powder Bed Fusion
PGT = Princeton Gamma Tech
PSD = Particle Size Distribution
SBM = Stirred Bead Milling
SEM = Scanning Electron Microscope

Symbols

CDC = Darvan C solid mass concentration [mg.m-2]
E_m = Specific energy [$kJ.kg^{-1}$]
K = Consistency index [$Pa.s^n$]
n = Flow behavior index [−]
t = Process duration [s]
V_r = Stirrer speed [$m.s^{-1}$]
w_{HA} = Solid mass fraction [−]
w_p: w_{GM} = Powder/grinding media weight ratio
x_{50} = Median particle size [μm]
x_f = Final median particle size [μm]
x_{GM} = Grinding media size [μm]
x_i = Initial median particle size [μm]
YSZ = Yttria-stabilized zirconia
α = Acceleration [$m.s^{-2}$]
γ = Shear rate [$1.s^{-1}$]
η = Viscosity [Pa.s]
ρ_{GM} = Grinding media density [$kg.m^{-3}$]
τ = Shear stress [Pa]
φ_{GM} = Beads filling degree [−]

There is a variety of works in the literature using different methods to perform the comminution of HA powders to reduce their particle size (Table 1). Kwade et al. [24] pointed out the interest of having a large number of stress events and stress intensity in a stirred bead milling (SBM) process compared to those present in other ball-milling processes (mechanical, tumbling, vibrating, high energy ball mills …). The grindability of materials is not so easy to evaluate concerning ultrafine wet grinding processes, so according to the recent review analysis by Taylor et al. [25], the most practical method to define optimum conditions and specific energy requirements for a stirred bead milling process is to perform tests on a laboratory-scale mill.

Table 1
Report of previous bibliographic studies on the grinding of hydroxyapatite powders using different milling processes. N/A will be written when data was not indicated by the authors in the publication. (w_p:w_{GM} = powder/grinding media weight ratio, x_{GM} = grinding media size, x_i = initial median particle size, x_f = final median particle size).

No.	Reference	Kind of mill, wet or dry conditions	Operating conditions	Crushed material, initial and final particle sizes
1	[26]	Agitator bead mill, wet	t = 1 h, w_p:w_{GM} = N/A x_{GM} = 200 μm, zirconia beads, additive BYK 151	Si, Ti, HA (Alfa aesar), x_i = <44 μm, x_f = 0.1 μm
2	[27]	Vibration ball milling, high-energy ball milling, dry	t = 1 h, w_p:w_{GM} = 1:40 x_{GM} = N/A	HA (Wako, 99.5%), x_i = 250 μm, x_f = 0.1 μm
3	[28]	Ball milling, high-energy ball milling, dry	t = 1 h, w_p:w_{GM} = N/A x_{GM} = N/A inert atmosphere	Ti-20%HA, x_f ≈ 100 μm
4	[29]	Ball milling, dry	t = 3 h w_p:w_{GM} = N/A x_{GM} = N/A	Synthesized (Wet method) then calcinated HA, x_i ≈ 30 μm, x_f = 5 μm
5	[30]	Agitator bead mill, moliNEx system (Netzsch), wet	t = N/A, w_p:w_{GM} = N/A x_{GM} = 1850 μm, zirconia beads, water & ethanol	Synthesized (Wet method) then calcinated HA, x_i ≈ 30 μm, x_f = 5 μm
6	[31]	Agitator bead mill, moliNEx system (Netzsch), wet	t = 8 h, w_p:w_{GM} = N/A x_{GM} = 1850 μm, zirconia beads, ethanol/water	Synthesized (Wet method) then calcinated HA, x_i ≈ 30 μm, x_f = 1 μm (ethanol), x_f = 3–10 μm (water)
7	[32]	Shaker–mixer, tubular, dry	t = 3-6-24-96 h, w_p:w_{GM} = N/A x_{GM} = 2000 μm, zirconia beads	Calcium phosphate powders, x_i = 3 μm, x_f = 2–1.5-0.7-0.3 μm resp.

To summarize, our objectives were to find the SBM conditions able to produce highly loaded (HA solid mass fraction, ***w_{HA}*, equal to or higher than 0.50**) HA-filled slurries for their use as spray-drying process feedstock. They should contain dispersed particles with an ***x_{50}* in the range of 0.2 to 1.5 μm** and show a **viscosity lower than 0.1 Pa s** during the whole process. Between the wide range of parameter combinations, the optimal set, meaning **minimal energy consumption** to reach the same targeted powder properties, will be determined.

2. Material and methods

2.1. Materials

The starting stoichiometric HA powder used during the present study was produced by Urodelia (SA Company, Saint-Lys, France) via wet precipitation process (product reference 206.93.003). More details about the synthesis procedure can be found in a previous work [33]. Ultrapure water served as a dispersion medium in the suspensions prepared in this work. It was obtained from the equipment "Purelab Ultra" of VWS (UK) Ltd. Its density was found to be 0.9952 g cm^{-3} at 25 °C whereas its pH varied between 6.3 and 6.8 at 25 °C. A commercial dispersant Darvan® C (DC) was used for better stabilization of the prepared HA-filled slurries. It is an anionic polyelectrolyte (ammonium poly(methacrylate)) provided by R. T. Vanderbilt Co. (Norwalk, CT, USA) consisting of an aqueous (clear to light amber) solution with an active matter concentration of 25 wt %. Producer specifications for this solution are a viscosity of 0.075 Pa s, a volumetric mass density of 1.11 ± 0.02 g cm^{-3}, a pH of 7.5–9, and an average molecular weight of 10, 000 to 16,000 Da, with a low tendency to foam.

2.2. Characterization of HA powders and HA-filled slurries

2.2.1. Particle size distributions and morphology

The PSD of the starting HA powder and HA-filled ground suspensions collected during the SBM process was determined by laser diffraction method (Mastersizer MS3000 Malvern Panalytical). A total number of replicate measurements (N) of five was performed for each suspension to calculate the resulting sample mean and sample standard deviation. In the following, the information on the number of measurements, the mean value and the standard deviation will be given as follows: (N = 5, mean ± standard deviation). Refractive indices of 1.632 and 1.330 were used for HA particles and water, respectively, and a particle absorption index of 0.1. For dry powders, a venturi pressure of 0.1 bar was used for the measurement. Fig. 1a shows the PSD of the starting dry HA powder, which has an x_{50} of 21.2 ± 1.6 μm. Initial and ground powder morphologies were investigated by scanning electron microscopy (LEO 435 VP) equipped with a Ge detector (Imix-PC, PGT). In the case of the ground powders, the slurries were freeze-dried overnight and the resulting dry powder was metallized with a thin film of silver using a Scancoat Six sputter coater. Fig. 1b shows the scanning electron microscope (SEM) micrographs of the starting powder, it is composed of aggregates of smaller particles with irregular shape.

Powders specific surface areas were measured by nitrogen adsorption, following the Brunauer-Emmett-Teller (BET) method. A Micromeritics® TriStar II Plus 3.00 equipment was used for the physisorption analysis of powders (N = 3, mean ± standard deviation). The specific surface area of the starting HA powder was found to be 0.8 ± 0.1 $m^2\,g^{-1}$. Ground powders were freeze-dried overnight before the measurement. All samples were previously degassed at 40 °C overnight in a VacPrep™ 061. The specific surface of ground powder was found to be 23.8 ± 6.0 $m^2\,g^{-1}$. This value will be used as a reference for the calculation of the dispersant concentration during the analyses.

The particle density of the starting HA powder was analysed by measuring the pressure change of helium in a calibrated volume in an AccuPyc 1330 Pycnometer (N = 10, mean ± standard deviation). The obtained true density of the initial powder was 3.10 ± 0.01 g cm^{-3}, close to the density of microscale hydroxyapatite powder reported in the literature (3.16 g cm^{-3}) [34].

2.2.2. Chemical and structural analyses

Fourier transform infrared spectroscopy (FTIR) analyses performed in a spectrometer Nicolet™ FTIR iS50 (Thermo Scientific™) were used to determine the chemical composition of the initial HA powder as well as the freeze-dried ground HA powder. KBr pellet method was used for the sample preparation.

X-ray diffraction (XRD) analyses of dry starting and ground HA powders were performed in a BRUKER's X-ray diffractometer D8 by using Cu Kα radiation (wavelength λ = 0.15406 nm) with a nickel filter at 40 kV and 40 mA. A step of 0.03° 2θ, and a time per step of 0.2 s were used to record the diffractograms in a 2θ range between 20° and 60° for the analysis and comparison of phase composition and crystallinity of powders. The dry powders were manually crushed using a mortar and pestle before measurement.

Analysis of the species produced due to the milling chamber and grinding media wear (Fe, Zr, and Y) during the SBM process was carried out by inductively coupled plasma atomic emission spectrometry (ICP-AES, Ultima2R HORIBA). Slurry aliquots collected during and after the SBM process were freeze-dried to obtain a dried powder. One gram of each sample was accurately weighed and introduced in a mineralization tube, then dissolved by acid digestion, adding 12 ml HNO_3 65%, 3 ml HCl 36.5–38%, and 2 ml ultrapure water, and then heated at 95 °C during 1 h. After cooling, ultrapure water was added to all solutions until a total of 50 ml before being injected into the plasma. One of the three SBM runs analysed (Table 2-Run 2) was performed and analysed three times to obtain the mean value and the standard error of the measurement.

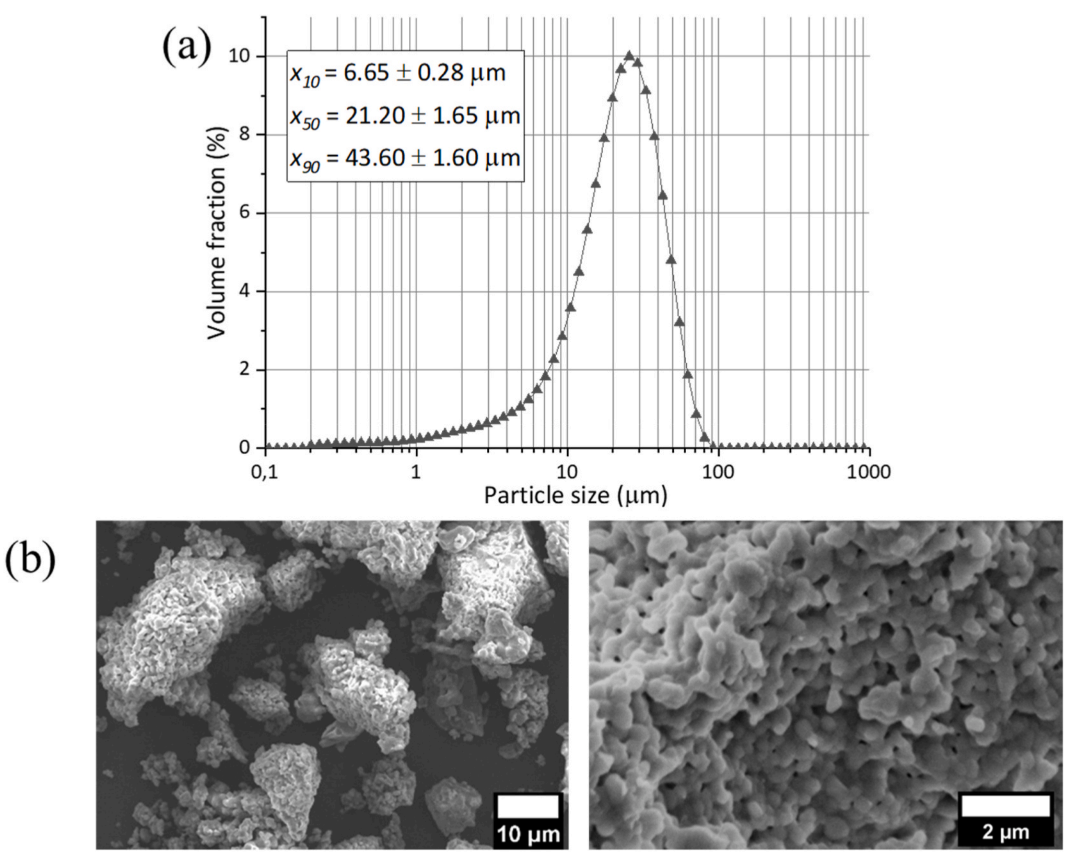

Fig. 1. (a) PSD and (b) SEM micrographs of as-received hydroxyapatite powder.

Table 2
List of experiments performed, including the experimental conditions (DC dosage respect to the ceramic specific surface), final specific energy, particle size obtained at the end, and purpose of the run. * Run was performed three times for the repeatability study.

Run no.	x_{GM} [mm]	φ_{GM} [−]	V_r [m. s^{-1}]	w_{HA} [−]	DC dosage [mg. m^{-2}]	Grinding time [min]	Ending E_m [kJ. kg^{-1}]	x_{10} [μm]	x_{50} [μm]	x_{90} [μm]	Operating condition studied
1	0.6	0.85	7.7	0.20	0	120	2880	0.6 ± 0.1	1.7 ± 0.2	3.7 ± 0.8	DC dosage
2*	0.4	0.75	5.7	0.20	2.1	120	5760	0.3 ± 0.1	0.4 ± 0.1	0.6 ± 0.1	V_r
3	0.4	0.75	3.8	0.20	2.1	135	3240	0.4 ± 0.1	0.7 ± 0.1	2.6 ± 0.5	
4	0.4	0.75	11.5	0.20	2.1	15	1800	0.4 ± 0.1	0.6 ± 0.1	0.9 ± 0.1	
5	1.0	0.85	7.7	0.10	2.1	60	2571	0.5 ± 0.1	0.9 ± 0.1	2.6 ± 0.2	x_{GM}
6	0.4	0.85	7.7	0.10	2.1	60	1600	0.4 ± 0.1	0.6 ± 0.1	1.0 ± 0.1	
7	0.4	0.75	11.5	0.10	2.1	7	3360	0.3 ± 0.1	0.5 ± 0.1	1.4 ± 0.1	w_{HA}
8	0.4	0.75	11.5	0.30	2.1	15	1714	0.5 ± 0.1	0.8 ± 0.1	1.8 ± 0.1	
9	0.4	0.75	11.5	0.50	2.1	15	720	0.5 ± 0.1	0.9 ± 0.1	2.0 ± 0.1	
10	0.4	0.75	5.7	0.50	2.1	120	654	0.5 ± 0.1	0.9 ± 0.1	2.1 ± 0.1	PSD evolution with grinding time
11	0.6	0.85	7.7	0.30	2.1	60	720	0.4 ± 0.1	0.9 ± 0.1	2.3 ± 0.4	

2.2.3. HA-filled slurries rheological and electrophoretic measurements

A TA Instruments AR2000 rheometer equipped with a temperature control Peltier plate was used for the rheological analysis of the HA-filled suspensions. A 40 mm crosshatched parallel plates system and a gap between plates of 1300 μm were chosen as configuration. Such geometries with rough surfaces were preferred to avoid sliding effects and a rapid radial migration of the suspended solids when using a cone-plate system. In addition, the gap of 1300 μm was chosen for being at least 10 times higher than the largest particle size understudy, which corresponds to an x_{50} of 100 μm in the starting HA powder, thus also avoiding wall effects [35]. To produce the flow curve of each sample a constant plate temperature of 25 °C and an increasing shear rate (steady-step flow step) were used taking ten points by decade. A conditioning step was applied before the measurements at a shear rate of 200 s^{-1} during 30.0 s and an equilibration time of 30.0 s. At least three measurements of each slurry were performed to obtain the standard error of the mean.

Even though prepared suspensions are intended for a posterior spray-drying process with typically high shear rates (10^5 to 10^6 s^{-1}), the step of the process that could bring more handling problems (due to a higher viscosity) is during the pumping and mixing of the suspensions, which produce lower shear rate (10 to 10^3 s^{-1}) [36]. Although the geometry used allows for high accuracy measurements, a practical limitation is the lowering of the highest shear rate limit that some samples can reach before being ejected out of the gap due to centrifugal forces. For this reason, the suspensions were compared over an equal shear rate range of 10–100 s^{-1}.

The influence of different w_{HA} and DC dosages on the rheological behaviour of ceramic suspensions was investigated. HA slurries were prepared by gradually pouring the corresponding amounts of DC and initial HA powder (before milling) in water. Samples with a total volume of 20 ml were stirred at 600 rpm for 10 min to ensure the homogeneity of the suspensions before the rheological analyses. No significant differences in the dispersion state were observed when applying sonication to the suspensions.

Several rheological mathematical models are usually applied to rheograms to transform them into the information of the steady shear fluid rheological behaviour. In this work, the Herschel-Bulkley model (Equation (1)), which is a three-parameter rheological model describing a non-Newtonian fluid, was used to fit the data.

$$\tau = \tau_y + K(\dot{\gamma})^n \tag{1}$$

where τ is the shear stress [Pa], τ_y the yield stress [Pa], $\dot{\gamma}$ the shear rate [s^{-1}], K the consistency index [Pa.s^n], and n the flow behaviour index [−].

The stabilization of a suspension may be evaluated by the zeta potential of the suspended particles. The potential is the electrical potential difference between the particle surface and the liquid beyond the ion charge cloud. The zeta potential of HA particles in slurries containing different concentrations of DC dispersant was determined by electrophoretic mobility using a Zetasizer Nano-ZS (Malvern Panalytical) at 25 °C. Different samples of 20 ml at $w_{HA} = 0.20$ were prepared by adding the corresponding HA powder amount and different dosages of DC (active component) from 0 to 2.1 mg m^{-2} to the ceramic powder surface (0–5 wt % to the ceramic mass) before being stirred for 2 h. Samples were diluted before the analysis to avoid the multiple diffusion phenomena and adjusted to a solids concentration of 4 mg mL^{-1}. Each zeta potential value reported was calculated from the mean of five measurements as well as the standard error.

The pH of the water and HA-filled suspensions was measured by Hach Sension + PH3 Basic laboratory pH meter, which was calibrated with standards pH 4, 7, and 10 each time before the repetition of at least five different measurements. The pH of an HA-filled suspension at $w_{HA} = 0.50$ was found to be 9.5 ± 0.2 at 25 °C due to the basic properties of HA particles. Padilla et al. [37] already offered a study of the influence of the pH and dispersants on the zeta potential of HA particles. They found that the most constant and highest zeta potential values were always obtained at pH ≥ 8. For this reason, no further analyses neither alteration of the pH of the HA-filled suspensions was followed during our study.

2.3. Stirred bead milling (SBM) experiments

Several SBM runs (Table 2) were carried out in commercial equipment Labstar manufactured by NETZSCH (Germany) to reduce the size of the HA particles present in the slurries. For each experiment, firstly, the suspension was prepared in a stirrer tank before being pumped to the milling chamber. The corresponding dispersant agent DC volume was added to water followed by the addition of the weighted HA powder amount. The total batch size was approximately 2 kg for each of the runs. All dispersions were agitated for 10 min at 600 rpm at 25 °C before starting the pumping and grinding process. The duration of the run and the DC and HA amounts used at each run are indicated in Table 2.

A detailed scheme of the experimental setup is provided in a previous work [38]. This SBM Labstar equipment is a laboratory-scale model with a grinding chamber volume of 0.62 l. The horizontal configuration of this circulation Zeta® grinding system ensures uniform exposure of the product through the media-intensive grinding zone within the mill as well as a high product throughput rate. A pin grinding system, of 7.2 cm in diameter, as a media mill stirrer, provides a high grinding intensity while a multi-zone cooling system prevents overheating of the product. The equipment has a stirrer speed (V_r) limit range of 1000–4000 rpm corresponding to a tip stirrer speed range of 3.8–17.3 m s^{-1}. The bead wear was reduced by using high resistant Yttrium Stabilized Zirconia 95% (YSZ, ZrO_2) micro grinding beads (Zirmil® Y from WAB-Group) (bead density ρ_{GM} = 6020 kg m^{-3}). Different grinding media sizes (x_{GM}) were used to study their effect on the final product quality. The nominal and laser diffraction measured x_{GM} values for the grinding media used are described in Table 3. Refractive and absorption indices of 2.148 and 1.000 respectively were used for the measurements.

Once comminution has occurred in the grinding chamber, the dispersion leaves through a steel (Cr–Ni-steel) separating cartridge of 100 μm installed at the outlet of the grinding chamber to separate the product returning to the feeding tank and keep the beads inside the chamber. In this way, the circulation mode (multi-passes) was selected as the operating mode. The product flow rate was kept constant at 8.8 × 10^{-6} m^3 s^{-1} and its analysis was kept out of the scope since it was already demonstrated that it does not have a significant effect on the product quality [39].

According to the literature [40,41], the specific energy (E_m) is more relevant than the grinding time to quantify the effect of operating parameters in SBM processes to reach a certain product fineness. E_m is the ratio of the total energy supplied to the grinding chamber to the mass of solid processed. The determination of E_m for a demanded product quality also depends among others on the mode of the milling operation [42]. Details on its calculation can be found in a previous experimental study [39]. Briefly, for a grinding process following a circulation or recycling mode, E_m can be determined as follows:

$$E_m(t) = \frac{E(t)}{m_p} = \int_0^t \frac{(P(\tau) - P_0)d\tau}{m_p} \tag{2}$$

where m_p is the mass of the solid product, $P(\tau)$ is the power at the time τ and P_0 is the no-load power. During each run, the number of revolutions and torque were recorded by a torque sensor on the stirrer shaft, allowing the calculation of E_m.

3. Results and discussion

3.1. Initial suspension formulation

3.1.1. Influence of solid mass fraction (w_{HA}) on suspension viscosity

Fig. 2 shows the viscosity of the suspension at different w_{HA}. It can be observed that the higher the solid loading, the higher the slurry viscosity is, with a slight increase between w_{HA} = 0.40 and w_{HA} = 0.50 compared with the pronounced rise observed at w_{HA} = 0.55. Within a similar volume, the high solids content increases the resistance to gradual deformation by shear stress due to the higher number of entities with a reduced space to move. Suspensions exhibited a shear-thinning behaviour over the whole shear rate range, more pronounced on suspensions with higher concentrations. The suspension at w_{HA} = 0.50 showed the most suitable behaviour as a highly loaded suspension in terms of experimental handling for the SBM process and the subsequent spray-drying process. This concentration was kept constant for the rest of the work. Suspensions with w_{HA} higher than 0.55 showed handling difficulties and adverse phenomena produced by the suspension instability, such as sedimentation. For this reason, it was not possible to perform their measurement.

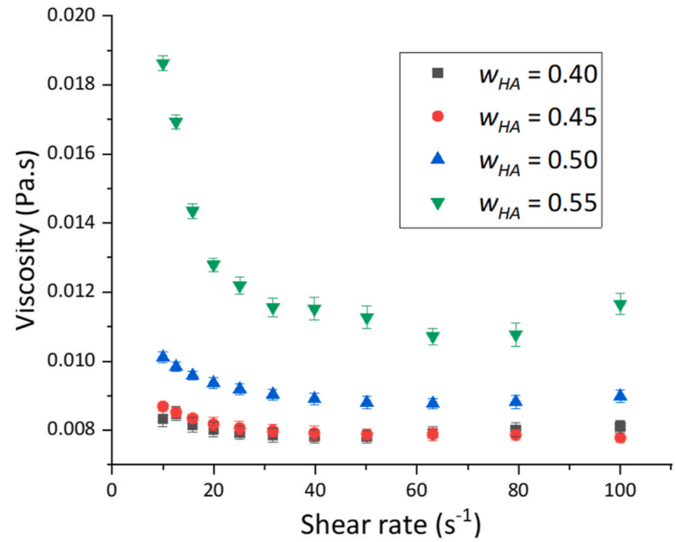

Fig. 2. Viscosity-shear rate curves obtained for several suspensions containing different solid mass concentrations.

The shear-thickening behaviour observed at a high shear rate for the samples with higher concentrations will be also observed in the next rheological analyses although our explanation will be only offered in this section. This phenomenon was already observed by Bergström [43] in his study on the rheological behaviour of concentrated ceramic suspensions. He observed that concentrated aqueous silicon carbide suspensions showed a strong, sometimes discontinuous, shear thickening. He attributed this behaviour to a possible hydrodynamic clustering, where anisotropic particles will be strongly affected by flow changing the suspension structure. Thus, altering the resistance to flow at some critical shear rate. This shear thickening behaviour seemed to increase with the suspension concentration. This transition to shear-thickening is sample-specific and other factors like particle size (distribution) and particle shape may control it [44].

3.1.2. Dispersing agent content

The amount of dispersing agent DC needed to obtain well-stabilized suspensions was determined through different preliminary analyses.

First, the zeta-potential evolution of the initial HA particles in an aqueous suspension was analysed. The changes in the zeta potential at different DC concentrations can be observed in Fig. 3a. In the range studied, a concentration ≥2.1 mg m^{-2} of DC the zeta-potential value exceeded the targeted limit of −30 mV, thus indicating that there is a sufficient number of negatively charged particles that could trigger their repulsion and prevent the flocculation. The pH of the measured samples was 9.5 ± 0.2 at 25 °C, as previously explained it was attributed to the basicity of HA particles. The different concentrations of DC tested did not show any significant alteration of the pH measured.

Secondly, the influence of the dispersant DC concentration on the x_{50}

Table 3
Vendor provided nominal and measured grinding media sizes. The measured values show the average and the standard deviation obtained from three measurements.

Nominal x_{GM} value *(mm)*	Measured x_{10} value *(mm)*	*Measured* x_{50} value *(mm)*	*Measured* x_{90} value *(mm)*
0.35–0.45 (0.4)	0.32 ± 0.01	0.39 ± 0.01	0.45 ± 0.01
0.6	0.55 ± 0.01	0.71 ± 0.01	0.93 ± 0.01
1.0	0.76 ± 0.01	1.15 ± 0.01	1.85 ± 0.03

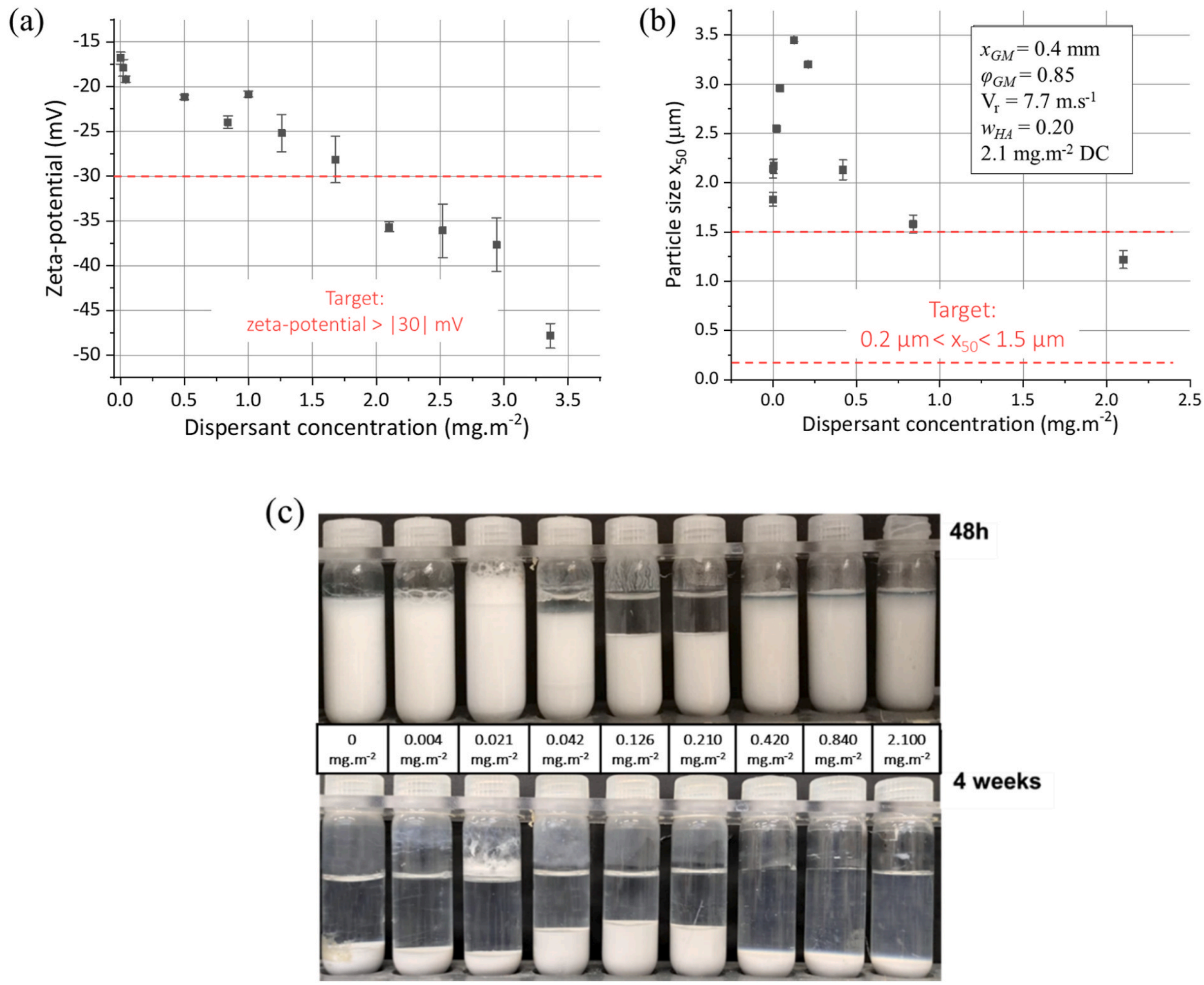

Fig. 3. Effect of DC concentration on the (a) suspended particles zeta potential, (b) powder median size (x_{50}) and (c) the settlement after 48 h and after 4 weeks of a slurry ground at $E_m = 2880$ kJ kg^{-1} with a HA solid mass fraction of 0.20.

of the HA particles in a ground suspension (Table 2– run 1) at $w_{HA} = 0.20$ was evaluated. The evolution of the x_{50} of the HA particles at different DC concentrations is shown in Fig. 3b. For concentrations higher than 0.84 mg m^{-2} of DC, the x_{50} of ground particles was reduced until it entered in our targeted range of particle size values (0.2 μm < x_{50} < 1.5 μm) at a DC dosage of 2.1 mg m^{-2}. An initial increase of the particle size is noticed at low dispersant concentrations, which leads us to hypothesize that a particle-binding bridge process between the HA particles is taking place due to an insufficient dispersant covering degree, leaving free surface sites exposed to interaction. Then, by increasing the dispersant concentration, the coverage is increased and the repulsion of the particles could be triggered. The third study was the evaluation of the sedimentation behaviour of these suspensions, which contain different DC dosages. The suspensions were magnetically stirred for 10 min and different aliquots of 10 ml of suspension were poured into nine different test tubes. To evaluate the sedimentation behaviour, photographs of the tubes after 48 h and after 4 weeks were taken for comparison (Fig. 3c). It can be observed how at very low DC concentrations the sedimentation behaviour shows minor changes compared with the absence of dispersant. Instead, for the concentration range from 0.042 to 0.21 mg m^{-2} faster sedimentation is observed, and at the end of the experiment, the final sedimentary volumes of these samples were more important than for the rest of the tubes. It is indicative of the dispersion state. When the interparticle forces are highly attractive, large and loose-packed flocs are formed, resulting in a more important and less dense sedimentary volume [20]. From a DC concentration of 0.42 mg m^{-2} the dispersant starts triggering the deflocculation of the particles showing a slower settling velocity and producing a minor but dense sedimentary volume. The stability of aqueous solutions of anionic polyelectrolyte dispersants has been largely explained in previous studies [45,46], describing how the dispersant dosage may affect the adsorbed layer conformation and hence the flocculation and stabilization of the suspensions containing HA particles.

The effect of the DC dosage on the rheological behaviour of the suspensions containing initial HA powder ($w_{HA} = 0.50$) was evaluated. The rheograms obtained can be observed in Fig. 4. It was observed that in presence of dispersant, the suspensions show a close to Newtonian behaviour over the studied shear rate, while the sample without dispersant showed a shear-thinning behaviour.

The first sharp decrease in viscosity is observed at low DC concentration (0.42 mg m^{-2}), then the viscosity tends to increase gradually as the DC concentration is increased beyond 0.42–2.10 mg m^{-2}. It is not easy to find a clear explanation for the mode of stabilization that could be due to steric interactions between the adsorbed DC layers and/or to electrostatic interactions, due to an increase in the surface charge.

To complete this study, the viscosity of the commercial DC (aqueous solution) was studied showing a higher viscosity than pure water (7.5 × 10^{-2} Pa s at 25 °C). The increase of viscosity at shear rate 100 s^{-1} with the concentration in a Darvan C-Water system was found to follow ($R^2 = 0.98$) the equation below:

$$\ln \eta = -5.03 + 0.12\, C_{DC} \tag{3}$$

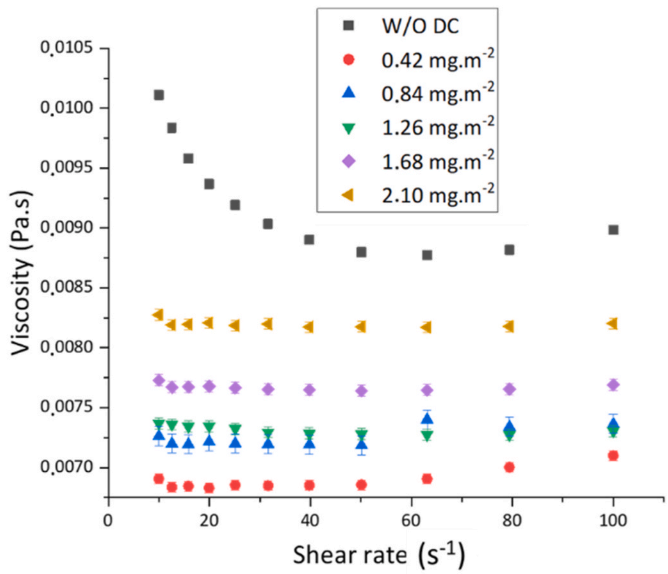

Fig. 4. Viscosity-shear rate curves obtained for several suspensions at w_{HA} = 0.50 before grinding process containing different dispersant DC concentrations.

Where η (Pa.s) is the viscosity of the system and C_{DC} ($mg.m^{-2}$) the DC concentration in an aqueous solution.

The relative viscosity of the suspensions (not reported here), obtained from the ratio between the viscosity of the suspension and the viscosity of the medium, for the different suspensions containing different amounts of DC, no longer shows an increase in viscosity when the DC concentration is increased beyond 0.42–2.10 mg m^{-2}. Thus, the observed increase in the viscosity of the HA-filled slurries when the DC concentration is increased, as shown in Fig. 4, can be simply explained by the increase in the viscosity of the medium. Thus, indicating that most of DC is not absorbed and remains in the solution. That can be explained by the lower specific surface area available in the initial HA particles (0.8 ± 0.1 m^2 g^{-1}) compared with the ground particles (23.8 ± 6.0 m^2 g^{-1}) obtained after the milling process for which the amount of DC was optimized.

3.2. Effect of grinding operating parameters

Firstly, the repeatability of the process for the particle size of the product obtained can be noted in Fig. S1 (supplementary material) where the mean value and standard error for the same run (Table 2 – runs 2) performed three times under identical conditions are reported.

To do not overextend the present paper the study of the impact of additional operational parameters was relegated outside of the scope. An example is the grinding media filling degree (φ_{GM}) which was settled to values between 75 and 85% of the total volume of the chamber for the experiments performed. It has been recently demonstrated by Guo et al. [47], using a vertical stirred media mill, that the PSD uniformity is generally independent of the φ_{GM}, although a higher φ_{GM} produces finer particle size at the same specific energy input. The increase of the grinding media filling rate increases in turn the collision frequency leading to a higher frequency of impacts on the material during the ball-ball collision [48].

3.2.1. Stirrer speed (V_r)

The rotation speed of a stirred mill is considered one of the most important factors affecting the grinding performance. It affects the collision intensity between beads, and hence the interactions with material particles to be ground. To study the influence of the stirrer speed on the SBM process results runs with different stirrer speeds (V_r=3.8, V_r = 5.7, and V_r = 11.5 m s^{-1}) were performed (Table 2 – runs 2, 3, 4) keeping the rest of the conditions identical between runs. These V_r correspond to 1000, 1500, and 3000 rpm respectively. Fig. 5a shows the evolution of the particle means size versus the grinding time. Increasing the stirrer speed increases the breakage kinetics and smaller particle size is reached for the same grinding time. This phenomenon agrees well with those reported on the impact of stirrer speed for YSZ beads; indicating that increasing stirrer speed results in a faster apparent breakage rate [49–51].

Fig. 5b shows the relation between the particle size x_{50} and the specific energy E_m at different stirring speeds V_r. If we compare both graphs 5a and 5 b, the difference of amplitude between curves is significant. It indicates that higher stirrer speed consumes lower energy to reduce the particle size until the desired product size. This observation differs from the observed in literature where the energy consumption increases at higher stirrer speed to reach a defined particle size. Indeed, for constant specific energies, the product becomes finer increasing the speed. It could be explained by the nature of the initial powder, which is composed of aggregates made of smaller particles [52]. The HA powder used in our study could then be defined as a weak material because of its capability to be ground [53]. When a certain value of specific energy is surpassed, the aggregates break rapidly into particles with a much smaller size than the initial aggregates. That could explain the verticality of the curves reaching relatively fast the final plateau in which adding higher energies does not decrease the particle size. Increasing the stirrer speed, the number of collisions and the stress intensity both increase however for weak materials the milling process depends more on the collision probability than the energy needed to break particles. Indeed, the supplied energy only needs to be at least equal to the required for the breakage of the aggregates. In addition, the operating time must be long enough for all aggregates to have the opportunity to be subjected to the stress of beads or the probability of collision must be boosted by increasing the stirrer speed [54].

A comparison of the whole size distribution at similar specific energies for the runs performed at different stirred speeds is shown in Fig. 6. At 660 kJ kg^{-1} (Fig. 6a), it can be observed how a contraction of the size distribution is more rapidly reached by increasing the agitation speed. For this E_m *value*, the PSDs of the suspensions show different grinding stages, being the grinding of suspensions from V_r = 3.8 m s^{-1} and V_r = 5.7 m s^{-1} still incomplete. It is not until higher specific energies (Fig. 6b) that the suspensions at lower stirrer speeds experience a PSD transformation from bimodal to unimodal to finally all suspensions have nearly similar PSDs reaching the complete grinding stage. The obtention of finer particle size at the same specific energy input supports the importance of using a higher stirrer speed for a more efficient and time-effective milling process. A similar tendency was observed in suspensions at w_{HA} = 0.50.

3.2.2. Grinding media size (x_{GM})

There are different factors to consider at the time of choosing the right type of grinding media like size, beads filling degree, contamination, cost, shape … depending on the application. The diameter of the grinding media will define the efficacy of the milling process since it can output diverse PSDs of the material supplied to the mill for the same duration. Tanaka [55] derived an empirical equation to calculate the optimum diameter in ultrafine wet milling processes under given conditions (i.e. particle size and strength and ball or bead density and hitting speed). Since the inherent strength of the material is not precisely known, these indications cannot be easily applied but it gives one idea of the influence of bead size in a wet stirred milling process.

Two different mean grinding media sizes (x_{GM} = 1.0 mm and x_{GM} = 0.4 mm) were used on different runs (Table 2 – runs 5, 6) of the SBM process by keeping the rest of the operational parameters identical and the median particle sizes and PSDs obtained are compared in Fig. 7. For a given specific energy, faster production of finer particle size and a monomodal distribution occurs when using x_{GM} = 0.4 mm, thus yielding a different product quality. A similar decrease in the median particle size

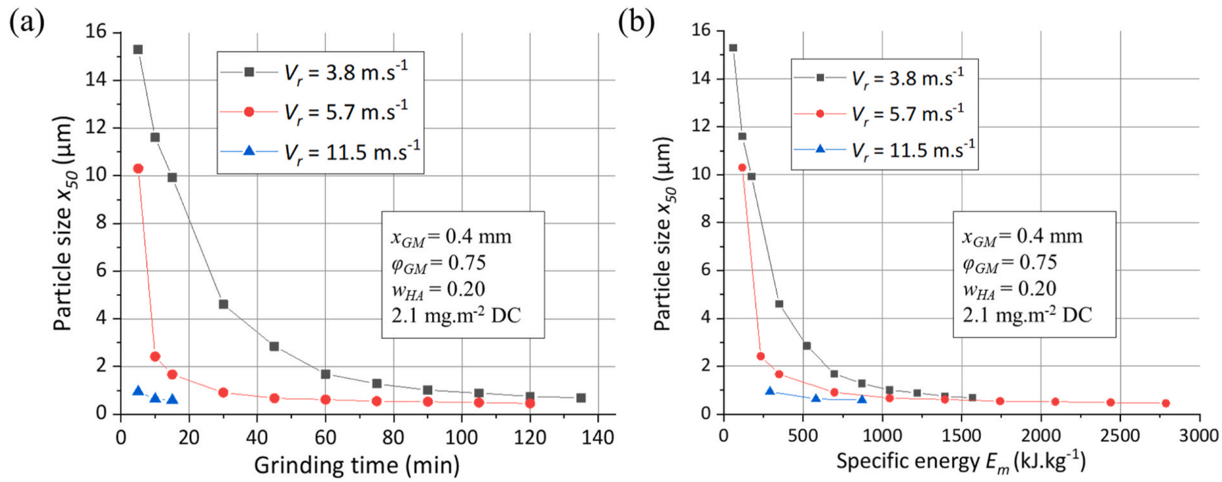

Fig. 5. Influence of stirrer speed on SBM product quality. a) Particle mean size versus grinding time. b) Particle mean size versus specific energy.

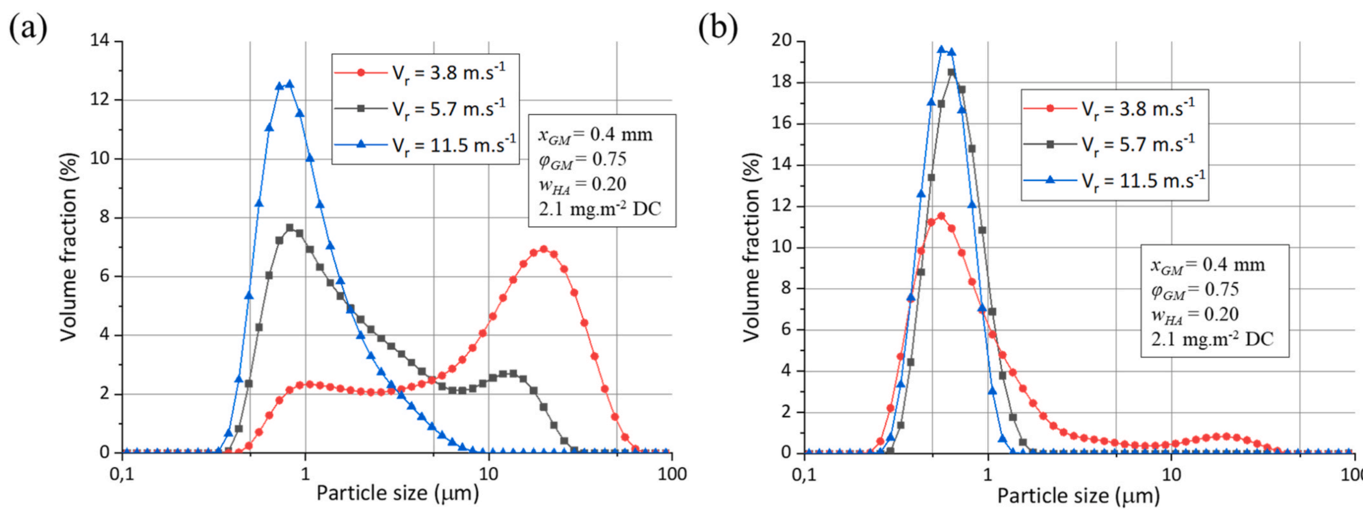

Fig. 6. (a) Effect of stirrer speed on the PSD of ground suspensions at 660 kJ kg^{-1}. (b) PSD of ground suspensions at the moment of obtaining uniform and unimodal distribution, equivalent to 3240 kJ kg^{-1}, 2160 kJ kg^{-1}, and 1800 kJ kg^{-1} for V_r = 3.8 m s^{-1}, V_r = 5.7 m s^{-1}, and V_r = 11.5 m s^{-1} respectively.

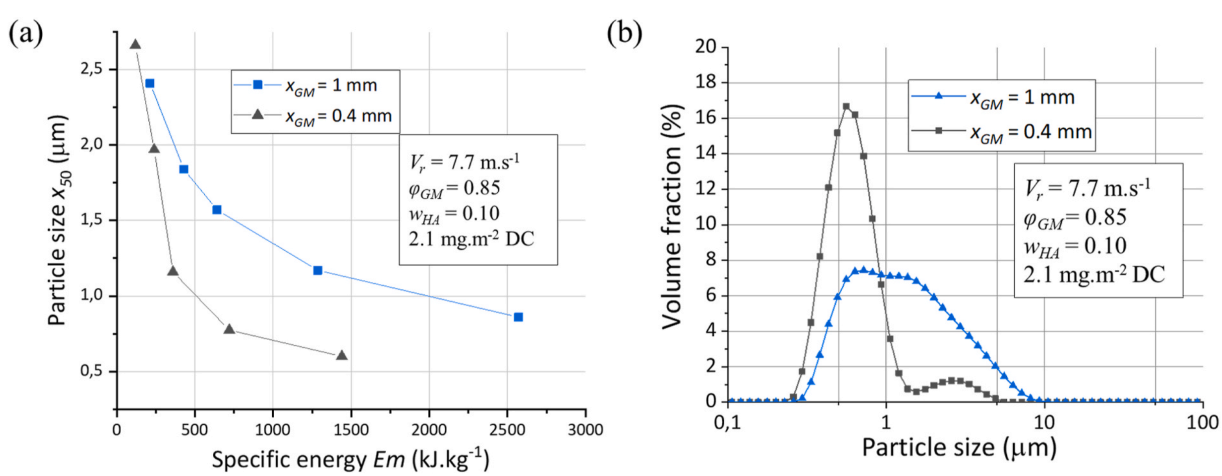

Fig. 7. Effect of the (YSZ, ZrO_2) grinding media size on the (a) particle median size and (b) PSD (x_{GM} = 1 mm and 0.4 mm, at 1350 kJ kg^{-1}) of a hydroxyapatite slurry during the stirred bead milling process. Each distribution is the average of five measurements on the same sample.

and the width of the size distribution decreasing the bead size was also reported on TiO_2 dispersion [56] while a quite different effect was observed on the grinding of talc [52]. For the talc which is a lamellar material, the minimum fineness was reached for intermediate bead size, and an increase in the width of the distribution was obtained using the largest beads. More recently, Li et al. [57] concluded that optimal bead size decreased upon an increase in the stirrer speed. It was explained by the two counter-acting effects of bead size: more bead-bead collisions (more stressing events) with less energy/force (lower stress intensity) upon a decrease in bead size. Strobel et al. [58] also observed that the bead size affects the flow pattern of the suspension through the milling chamber. They found that for a small bead size (0.5 mm in their study), different milling bead packing densities arise in the mill chamber resulting in different flow rates through those zones. The suspension evades regions with high bead concentrations inside the mill. It results in a large fraction of non-stressed particles and at the same time many impacts on stressed particles which could help to explain the multimodal profile of the PSDs.

3.2.3. Solid mass fraction (w_{HA})

A comparison of the effect of the suspension solid concentration on the quality of the product during the milling process is shown in Fig. 8. To analyse this effect, runs (Table 2 – runs 7, 8, 9) with different concentrations ($w_{HA} = 0.10$, $w_{HA} = 0.30$, and $w_{HA} = 0.50$) were performed keeping the rest of the conditions (V_r, x_{GM}, DC dosage …) identical between runs. This w_{HA} range ($w_{HA} = 0.10$ to $w_{HA} = 0.50$) comprises all concentrations used during the runs carried out for the present study.

Fig. 8a shows the evolution of the particle mean size (x_{50}) versus the grinding time. It is observed that for the same process duration finer mean particle size is obtained when the solid concentration is lower. However, when comparing the particle mean size versus the specific energy, the effect of the solid concentration can be truly followed. It can be deducted that for an equal specific energy input spent, the higher is the load of the suspension the finer is the mean particle size obtained. It indicates that a higher process energy efficiency is reached in highly loaded suspensions. Similar results were observed on the dispersion of TiO_2 [56] but an opposite effect was reported on other materials [38,58] for which an inverse proportion between milling efficiency (capturing efficiency of the product particles by milling beads collisions) and suspension viscosity was observed. In the present study, such an effect was not noticeable. It could be explained by the smaller difference magnitude between suspensions viscosities (cf. next section) within the w_{HA} range in our work compared with the above-mentioned studies.

We could then conclude that the importance of the control of the suspension formulation (Darvan C dosage, and HA solid mass fraction) and the operational conditions of the mill (stirrer speed, grinding media size, …) has been proved through the studies performed in Sections 3.1 and 3.2. In addition, we were able to adjust these conditions to tune the final HA particles properties. Highly loaded stabilized suspensions with finely ground HA particles in an x_{50} range of 0.2–1.5 μm could be prepared for its use as suspension feedstock in a spray-drying process.

A wide range of operating parameters gave a product meeting the targeted characteristics; however, it was demonstrated that by using a faster stirrer speed ($V_r = 11.5$ m s^{-1}), smaller grinding media size ($x_{GM} = 0.4$ mm), and higher solid concentration ($w_{HA} = 0.50$) is possible to reduce the energy consumption in the process reaching a higher energy efficiency.

3.3. Characterization of slurries and powder products

3.3.1. Physico-chemical properties of ground powders

Fig. S3 shows the XRD and FTIR spectra of ground powders (Table 2 – runs 6, 10 respectively) to the initial powder. Through the XRD analysis (Fig. S3a) of the powders, the maintenance of the calcium phosphate phase (stoichiometric hydroxyapatite (JCPDS 00-009-0432)) and crystallinity state can be verified as unaltered, as well as no secondary phases were detected [5]. The FTIR analysis (Fig. S3b) also confirmed the absence of relevant changes in the chemical composition of the HA powder after the SBM process. The vibration bands corresponding to PO_4 are visible at 1092 cm^{-1}, 1040 cm^{-1}, 962 cm^{-1}, 601 cm^{-1}, 575 cm^{-1}, 561 cm^{-1}, as well as the band belonging to OH^- at 650 cm^{-1} and 3600 cm^{-1} [5,59]. The band at 1400 cm^{-1} was attributed to the vibration band from C–H bending from the methacrylate backbone of the dispersant DC [60]. Whether or not the presence of DC affects the posterior spray-drying step is detailed in another paper [22].

SEM micrographs of the freeze-dried powder after the SBM process (Table 2 – run 5) are shown in *Figure S2*. The size of the particles observed would confirm the PSD measured by laser diffraction. The ground (2.97 ± 0.01 g cm^{-3}) and initial powder (3.10 ± 0.01 g cm^{-3}) densities were measured with no clear alteration between them. Only a slight difference which was attributed to the measurement accuracy of the equipment used.

The chemical analysis of the product with ICP-AES equipment allowed us to characterize accurately the presence of species coming from the grinding chamber and grinding media wear. It is known that grinding media wear can be minimized by applying optimal media diameter, specific energy input, and stirrer speed [61]. The species analysed were Fe, Zr, and Y, and an example of how an operational parameter, such as the stirrer speed V_r, can influence its production is illustrated in Fig. 9. To reach the same particle size, three different runs (Table 2 – runs 2, 3, 4) were performed at three different speeds (3.8, 5.7, and 11.5 m s^{-1}), then samples were collected at different times (135

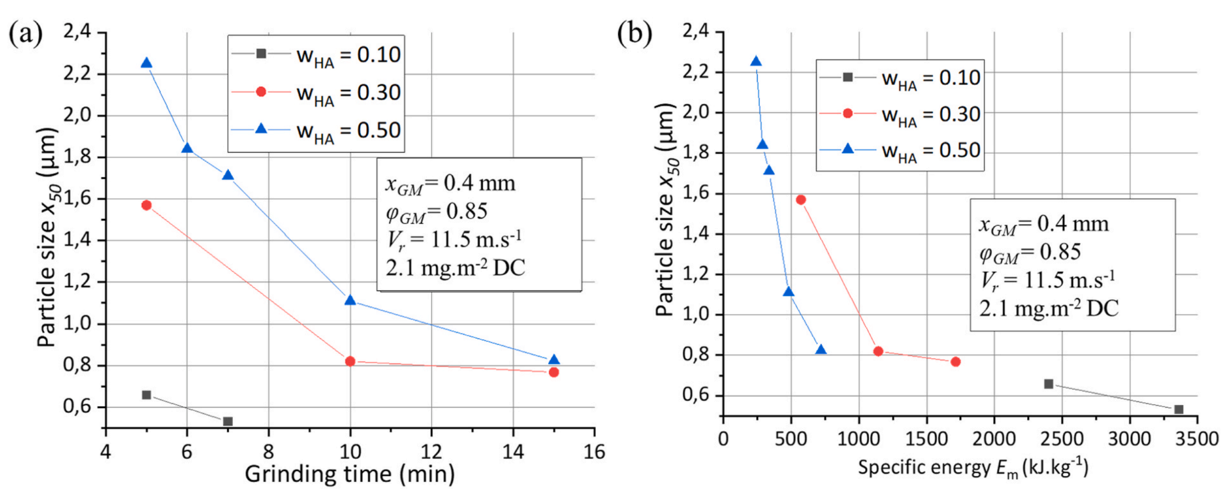

Fig. 8. Influence of w_{HA} on SBM product quality. a) Particle mean size versus grinding time. b) Particle mean size versus specific energy.

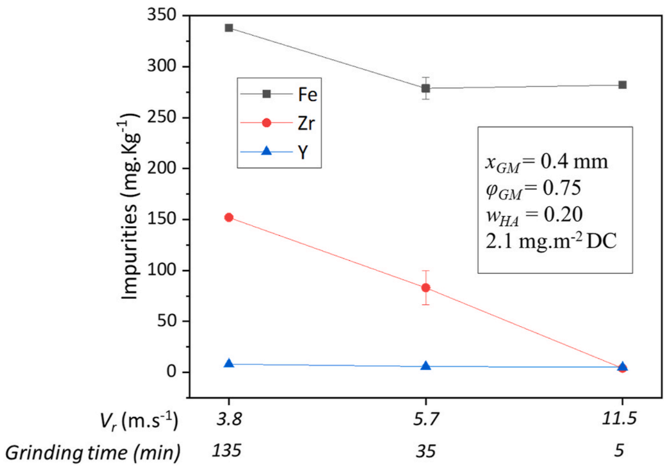

Fig. 9. ICP-AES elemental analysis of Fe, Zr, and Y of the final product obtained by three different SBM process runs (Table 2– runs 2,3,4). Samples were collected once the same particle size objective ($\times_{50}$ = 0.8 μm) was reached.

min, 30 min, and 5 min, respectively) once an objective median particle size ($\times_{50}$ = 0.8 μm) was reached. As we mentioned before, one of the runs (Table 2 – runs 2) was performed three times under identical conditions to report the standard error and repeatability of the concentration of the species. In this study, the generation of the grinding media and chamber wear was minimized using the highest stirrer speed.

The presence of trivalent ions (e.g., Fe^{3+}) can have an important effect on suspension's rheology due to the interaction with anionic polyelectrolytes such as, Darvan C [62]. However, no further research was followed in this sense. Since, deeper study on the selection, operation and optimization of the process to minimize the grinding media wear and its effect was out of the scope of this paper. A wear reduction could be done by changing the material of the grinding chamber and stirrer, from stainless steel into ceramic or polymer, which is equally available commercially, avoiding or minimizing the generation of these species.

3.3.2. *PSD evolution with grinding time*

The evolution of the PSDs during SBM runs (Table 2 – runs 10, 11) with two different sets of parameters are shown as example in Fig. 10. Initial particle population having a median size of x_{50} = 21.20 μm experiments a gradual reduction during the SBM process. Final populations of micron and submicron particles can be obtained for different grinding times. In addition, a different combination of parameters can have diverse effects on the uniformity of the PSDs. SBM process parameters could be tuned to pursue a determinate PSD depending on the application.

3.3.3. *Rheological behaviour of the ground suspension*

The effect of the grinding time on the rheological behaviour of the suspensions was evaluated by taking aliquots at different times during an SBM process. The parameters of this SBM experiment (Table 2 – run 11) together with the rheograms can be observed in Fig. 11. A tendency of the rheological behaviour to turn into shear thinning with the grinding time was detected, therefore for a given solid concentration, this effect is more pronounced for suspensions with smaller particles. After 10 min of the process, an increase of the viscosity is observed at low shear rates with the increase of the grinding time (or decrease of the particle size). For a given solid mass fraction and the same volume, the smaller the particle size the higher the number of particles present. Thus, the particle surface area can be several orders of magnitude higher. Very small particles show Brownian motion acting against an applied shear force [63]. A clear shear-thinning behaviour is observed for the suspensions containing particles of smaller sizes. It could be due to a more favourable rearrangement of small particles to the flow direction. A higher grinding time increases the PSD span, increasing the maximum packing density as space can be filled more efficiently.

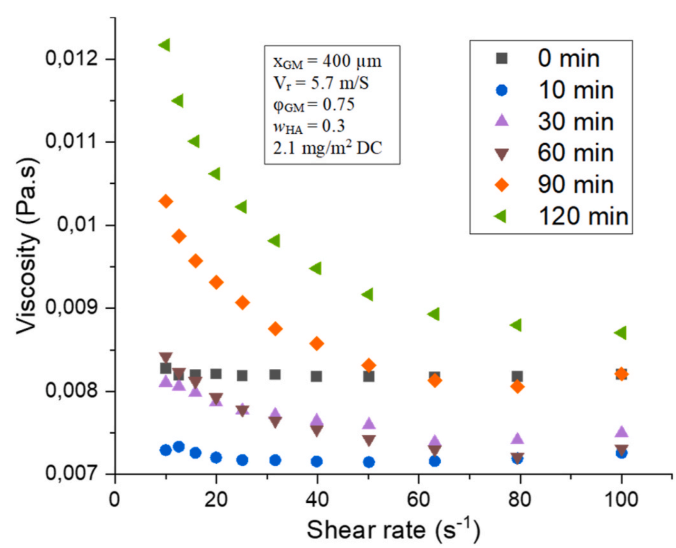

Fig. 11. The viscosity-shear rate curves obtained for suspensions ground at different grinding times (Table 2– run 11).

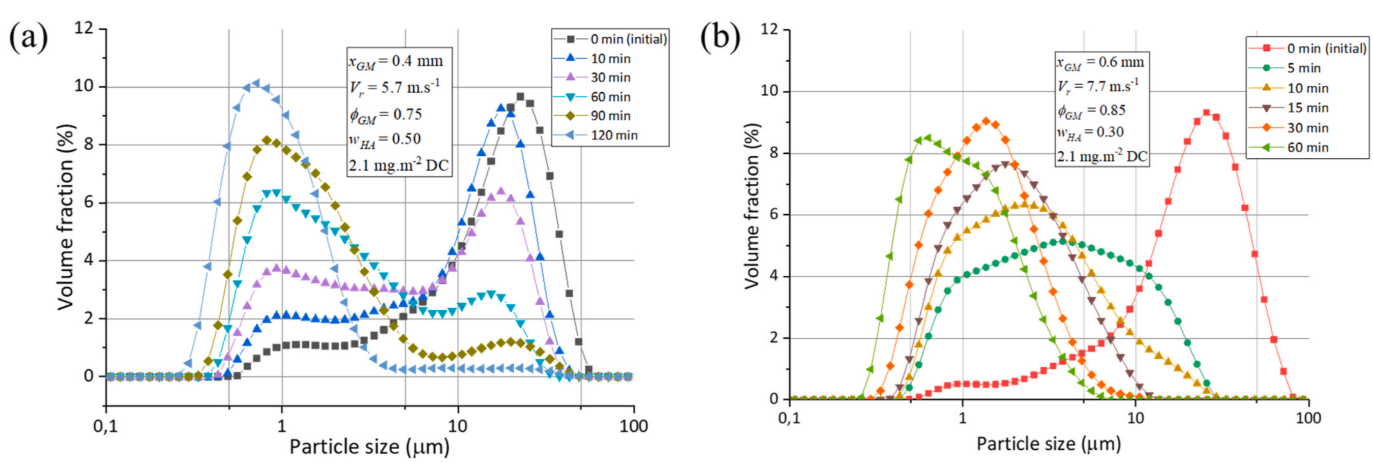

Fig. 10. Evolution of PSD of a HA slurry with the grinding time for two different sets of parameters. (a) run 10 and (b) run 11.

4. Conclusions

HA highly loaded suspensions were successfully ground and the additive DC was demonstrated to be an efficient dispersant additive altering the zeta potential of the particles and thus stabilizing the suspensions, better at a concentration of 2.1 mg m^{-2}. For this specific material, at the same specific energy values, faster stirrer speed ($V_r = 11.5$ m s^{-1}), smaller grinding media size ($x_{GM} = 0.4$ mm), and higher HA solid concentration ($w_{HA} = 0.50$) shorten grinding times obtaining finer particles. Indeed, the increase in stirrer speed showed a lower generation of grinding chamber and media wear during the process. The explanation for the low specific energy spent to perform the milling of the product comes from the weakness of the initial HA aggregates and the relatively low viscosities of the ground HA products even in fairly loaded suspensions. No significant increases in viscosity were observed for the suspensions in the conditions studied, thus keeping their processability.

The production of suspensions with characteristics and properties suitable for a subsequent spray-drying step ($w_{HA} \geq 0.50$; $x_{50} = 0.2$–1.5 μm; viscosity <0.1 Pa s) was possible by SBM process. And this was possible without major alteration of the composition or the structural phase of the initial HA product. As mentioned in the introduction, the utilization of these suspensions via the spray-drying process and the subsequent PBF additive manufacturing process was already explored [22,23].

The reduced specific energy cost and shorter processing time compared to other ball milling processes make SBM an attractive technique as a first step in the production of hydroxyapatite powder for PBF technologies.

Declaration of competing interest

The authors declare that they have no known competing financial interests or personal relationships that could have appeared to influence the work reported in this paper.

5. Acknowledgments

This project has received funding from the European Union's Horizon 2020 research and innovation programme under the Marie Skłodowska-Curie grant agreement No 764935.

We would like to express our acknowledgment to R. T. Vanderbilt Co. for the supplied Darvan C samples.

Appendix A. Supplementary data

Supplementary data to this article can be found online at https://doi.org/10.1016/j.ceramint.2022.05.149.

References

[1] C. Shuai, P. Li, J. Liu, S. Peng, Optimization of TCP/HAP ratio for better properties of calcium phosphate scaffold via selective laser sintering, Mater. Char. 77 (2013) 23–31, https://doi.org/10.1016/j.matchar.2012.12.009.
[2] S. Eosoly, D. Brabazon, S. Lohfeld, L. Looney, Selective laser sintering of hydroxyapatite/poly-ε-caprolactone scaffolds, Acta Biomater. 6 (2010) 2511–2517, https://doi.org/10.1016/j.actbio.2009.07.018.
[3] J.W. Lee, G. Ahn, D.S. Kim, D.-W. Cho, Development of nano- and microscale composite 3D scaffolds using PPF/DEF-HA and micro-stereolithography, Microelectron. Eng. 86 (2009) 1465–1467, https://doi.org/10.1016/j.mee.2008.12.038.
[4] L. Ferrage, G. Bertrand, P. Lenormand, D. Grossin, B. Ben-Nissan, A review of the additive manufacturing (3DP) of bioceramics: alumina, zirconia (PSZ) and hydroxyapatite, J. Australas. Ceram. Soc. 53 (2017) 11–20, https://doi.org/10.1007/s41779-016-0003-9.
[5] C. Rey, C. Combes, C. Drouet, D. Grossin, G. Bertrand, J. Soulié, Bioactive calcium phosphate compounds: physical chemistry, in: Reference Module in Materials Science and Materials Engineering, Elsevier, 2017, https://doi.org/10.1016/B978-0-12-803581-8.10171-7.
[6] Y. Xia, P. Zhou, X. Cheng, Y. Xie, C. Liang, C. Li, S. Xu, Selective laser sintering fabrication of nano-hydroxyapatite/poly-ε-caprolactone scaffolds for bone tissue engineering applications, Int. J. Nanomed. 8 (2013) 4197–4213, https://doi.org/10.2147/IJN.S50685.
[7] D. Grossin, A. Montón, P. Navarrete-Segado, E. Özmen, G. Urruth, F. Maury, D. Maury, C. Frances, M. Tourbin, P. Lenormand, G. Bertrand, A review of additive manufacturing of ceramics by powder bed selective laser processing (sintering/melting): calcium phosphate, silicon carbide, zirconia, alumina, and their composites, Open Ceramics 5 (2021), 100073, https://doi.org/10.1016/j.oceram.2021.100073.
[8] A. Lüddecke, O. Pannitz, H. Zetzener, J.T. Sehrt, A. Kwade, Powder properties and flowability measurements of tailored nanocomposites for powder bed fusion applications, Mater. Des. 202 (2021), 109536, https://doi.org/10.1016/j.matdes.2021.109536.
[9] H. Lu, X. Guo, Y. Liu, X. Gong, Effect of particle size on flow mode and flow characteristics of pulverized coal, KONA 32 (2015) 143–153, https://doi.org/10.14356/kona.2015002.
[10] L.X. Liu, I. Marziano, A.C. Bentham, J.D. Litster, E.T. White, T. Howes, Effect of particle properties on the flowability of ibuprofen powders, Int. J. Pharm. 362 (2008) 109–117, https://doi.org/10.1016/j.ijpharm.2008.06.023.
[11] X. Fu, D. Huck, L. Makein, B. Armstrong, U. Willen, T. Freeman, Effect of particle shape and size on flow properties of lactose powders, Particuology 10 (2012) 203–208, https://doi.org/10.1016/j.partic.2011.11.003.
[12] M.K. Stanford, C. Dellacorte, D. Eylon, Particle size effects on flow properties of Ps304 plasma spray feedstock powder blend, in: W.M. Kriven, H.-T. Lin (Eds.), Ceramic Engineering and Science Proceedings, John Wiley & Sons, Inc., Hoboken, NJ, USA, 2003, pp. 577–585, https://doi.org/10.1002/9780470294802.ch82.
[13] M. Schmid, F. Amado, G. Levy, K. Wegener, Flowability of powders for selective laser sintering (SLS) investigated by round robin test, in: P. da Silva Bártolo, A. de Lemos, A. Pereira, A. Mateus, C. Ramos, C. Santos, D. Oliveira, E. Pinto, F. Craveiro, H. da Rocha Terreiro Galha Bártolo, H. de Amorim Almeia, I. Sousa, J. Matias, L. Durão, M. Gaspar, N. Fernandes Alves, P. Carreira, T. Ferreira, T. Marques (Eds.), High Value Manufacturing: Advanced Research in Virtual and Rapid Prototyping, CRC Press, 2013, pp. 95–99, https://doi.org/10.1201/b15961-19.
[14] F. Erdem, The effect of binder on chemically precipitated hydroxyapatite during spray drying, Materiali in Tehnologije (2013) 4.
[15] A. Tsetsekou, C. Agrafiotis, I. Leon, A. Milias, Optimization of the rheological properties of alumina slurries for ceramic processing applications Part II: spray-drying, J. Eur. Ceram. Soc. 21 (2001) 493–506, https://doi.org/10.1016/S0955-2219(00)00232-6.
[16] P. Ramavath, R. Papitha, M. Ramesh, P. Babu, R. Johnson, Effect of primary particle size on spray formation, morphology and internal structure of alumina granules and elucidation of flowability and compaction behaviour, PAC 8 (2014) 93–99, https://doi.org/10.2298/PAC1402093R.
[17] J.S. Reed, J.S. Reed, Principles of Ceramics Processing, second ed., Wiley, New York, 1995.
[18] L. Pawlowski, P. Blanchart, Industrial Chemistry of Oxides for Emerging Applications, Wiley, Laboratory SPCTS, University of Limoges, France, 2018.
[19] R. Wisniewski, Spray drying technology review, in: 45th International Conference on Environmental Systems, 2015. Washington, https://ttu-ir.tdl.org/handle/2346/64598. (Accessed 14 August 2021).
[20] F. Garcia, N. Le Bolay, J.-L. Trompette, C. Frances, On fragmentation and agglomeration phenomena in an ultrafine wet grinding process: the role of polyelectrolyte additives, Int. J. Miner. Process. 74 (2004) S43–S54, https://doi.org/10.1016/j.minpro.2004.07.001.
[21] C. Onwulata, Encapsulated and Powdered Foods, first ed., 2005, https://doi.org/10.1201/9781420028300. Boca Raton.
[22] P. Navarrete-Segado, C. Frances, D. Grossin, M. Tourbin, Tailoring Hydroxyapatite Microspheres by Spray-Drying for Powder Bed Fusion Feedstock, Powder Technology, 2022, 117116, https://doi.org/10.1016/j.powtec.2022.117116.
[23] P. Navarrete-Segado, C. Frances, M. Tourbin, C. Tenailleau, B. Duployer, D. Grossin, Powder bed selective laser process (sintering/melting) applied to tailored calcium phosphate-based powders, Addit. Manuf. 50 (2022), 102542, https://doi.org/10.1016/j.addma.2021.102542.
[24] A. Kwade, Determination of the most important grinding mechanism in stirred media mills by calculating stress intensity and stress number, Powder Technol. 105 (1999) 382–388, https://doi.org/10.1016/S0032-5910(99)00162-X.
[25] L. Taylor, D. Skuse, S. Blackburn, R. Greenwood, Stirred media mills in the mining industry: material grindability, energy-size relationships, and operating conditions, Powder Technol. 369 (2020), https://doi.org/10.1016/j.powtec.2020.04.057.
[26] D. Holzmann, D. Holzinger, G. Hesser, T. Schmidt, G. Knör, Hydroxyapatite nanoparticles as novel low-refractive index additives for the long-term UV-photoprotection of transparent composite materials, J. Mater. Chem. 19 (2009) 8102–8106, https://doi.org/10.1039/B912116A.
[27] A.E. Hannora, A.S. Mukasyan, Z.A. Mansurov, Nanocrystalline hydroxyapatite/Si coating by mechanical alloying technique, bioinorganic chemistry and applications, 2012, https://doi.org/10.1155/2012/390104, 2012, 1-14.
[28] S. Tsipas, P. Goodwin, H.B. McShane, R.D. Rawlings, Effect of high energy ball milling on titanium-hydroxyapatite powders, Powder Metall. 46 (2003) 73–77, https://doi.org/10.1179/003258903225010523.
[29] R.T. Candidato Jr., P. Sokołowski, L. Łatka, S. Kozerski, L. Pawłowski, A. Denoirjean, Plasma spraying of hydroxyapatite coatings using powder, suspension and solution feedstocks, Przegląd Spawalnictwa. 87 (2015), https://doi.org/10.26628/ps.v87i10.491.

[30] R. Jaworski, C. Pierlot, L. Pawlowski, M. Bigan, M. Quivrin, Synthesis and preliminary tests of suspension plasma spraying of fine hydroxyapatite powder, J. Therm. Spray Technol. 17 (2008) 679–684, https://doi.org/10.1007/s11666-008-9220-2.
[31] R. Jaworski, C. Pierlot, L. Pawlowski, M. Bigan, M. Martel, Design of the synthesis of fine HA powder for suspension plasma spraying, Surf. Coating. Technol. 203 (2009) 2092–2097, https://doi.org/10.1016/j.surfcoat.2008.10.036.
[32] A. Bignon, J. Chevalier, G. Fantozzi, Effect of ball milling on the processing of bone substitutes with calcium phosphate powders, J. Biomed. Mater. Res. 63 (2002) 619–626, https://doi.org/10.1002/jbm.10379.
[33] M. Tourbin, F. Brouillet, B. Galey, N. Rouquet, P. Gras, N. Abi Chebel, D. Grossin, C. Frances, Agglomeration of Stoichiometric Hydroxyapatite: Impact on Particle Size Distribution and Purity in the Precipitation and Maturation Steps, Powder Technology, 2019, S0032591019308733, https://doi.org/10.1016/j.powtec.2019.10.050.
[34] Y. Wu, S. Bose, Nanocrystalline hydroxyapatite: micelle templated synthesis and characterization, Langmuir 21 (2005) 3232–3234, https://doi.org/10.1021/la046754z.
[35] H.A. Barnes, Measuring the viscosity of large-particle (and flocculated) suspensions — a note on the necessary gap size of rotational viscometers, J. Non-Newtonian Fluid Mech. 94 (2000) 213–217, https://doi.org/10.1016/S0377-0257(00)00162-2.
[36] N.J. Alderman, Non-Newtonian fluids: guide to classification and characteristics, ESDU Data Item 97034 (1997) 30.
[37] S. Padilla, Hydroxyapatite suspensions as precursors of pieces obtained by gelcasting method, J. Eur. Ceram. Soc. (2004) 10.
[38] M.A. Inam, S. Ouattara, C. Frances, Effects of concentration of dispersions on particle sizing during production of fine particles in wet grinding process, Powder Technol. 208 (2011) 329–336, https://doi.org/10.1016/j.powtec.2010.08.025.
[39] S. Ouattara, C. Frances, Grinding of calcite suspensions in a stirred media mill: effect of operational parameters on the product quality and the specific energy, Powder Technol. 255 (2014) 89–97, https://doi.org/10.1016/j.powtec.2013.11.025.
[40] A. Kwade, A stressing model for the description and optimization of grinding processes, Chem. Eng. Technol. 26 (2003) 199–205, https://doi.org/10.1002/ceat.200390029.
[41] S. Breitung-Faes, A. Kwade, Use of an enhanced stress model for the optimization of wet stirred media milling processes, Chem. Eng. Technol. 37 (2014) 819–826, https://doi.org/10.1002/ceat.201300686.
[42] A. Kwade, J. Schwedes, Chapter 6 wet grinding in stirred media mills, in: Handbook of Powder Technology, Elsevier, 2007, pp. 251–382, https://doi.org/10.1016/S0167-3785(07)12009-1.
[43] L. Bergström, Shear thinning and shear thickening of concentrated ceramic suspensions, Colloids Surf. A Physicochem. Eng. Asp. 133 (1998) 151–155, https://doi.org/10.1016/S0927-7757(97)00133-7.
[44] J.J. Stickel, R.L. Powell, Fluid mechanics and rheology of dense suspensions, Annu. Rev. Fluid Mech. 37 (2005) 129–149, https://doi.org/10.1146/annurev.fluid.36.050802.122132.
[45] T. Kuroiwa, I. Kobayashi, A.M. Chuah, M. Nakajima, S. Ichikawa, Formulation and stabilization of nano-/microdispersion systems using naturally occurring edible polyelectrolytes by electrostatic deposition and complexation, Adv. Colloid Interface Sci. 226 (2015) 86–100, https://doi.org/10.1016/j.cis.2015.09.003.
[46] K. Tong, X. Song, S. Sun, Y. Xu, J. Yu, The rheological behavior and stability of Mg(OH)2 aqueous suspensions in the presence of sodium polyacrylate, Colloids Surf. A Physicochem. Eng. Asp. 436 (2013) 1111–1120, https://doi.org/10.1016/j.colsurfa.2013.08.017.
[47] W. Guo, Y. Han, Y. Li, Z. Tang, Impact of ball filling rate and stirrer tip speed on milling iron ore by wet stirred mill: analysis and prediction of the particle size distribution, Powder Technol. 378 (2021) 12–18, https://doi.org/10.1016/j.powtec.2020.09.052.
[48] A. Kwade, J. Schwedes, Breaking characteristics of different materials and their effect on stress intensity and stress number in stirred media mills, Powder Technol. 122 (2002) 109–121, https://doi.org/10.1016/S0032-5910(01)00406-5.
[49] A. Afolabi, O. Akinlabi, E. Bilgili, Impact of process parameters on the breakage kinetics of poorly water-soluble drugs during wet stirred media milling: a microhydrodynamic view, Eur. J. Pharmaceut. Sci. 51 (2014) 75–86, https://doi.org/10.1016/j.ejps.2013.09.002.
[50] S.K. Singh, K.K. Srinivasan, K. Gowthamarajan, D.S. Singare, D. Prakash, N. B. Gaikwad, Investigation of preparation parameters of nanosuspension by top-down media milling to improve the dissolution of poorly water-soluble glyburide, Eur. J. Pharm. Biopharm. 78 (2011) 441–446, https://doi.org/10.1016/j.ejpb.2011.03.014.
[51] Y. Tanaka, M. Inkyo, R. Yumoto, J. Nagai, M. Takano, S. Nagata, Nanoparticulation of probucol, a poorly water-soluble drug, using a novel wet-milling process to improve in vitro dissolution and in vivo oral absorption, Drug Dev. Ind. Pharm. 38 (2012) 1015–1023, https://doi.org/10.3109/03639045.2011.637051.
[52] K. Ohenoja, M. Illikainen, Effect of operational parameters and stress energies on stirred media milling of talc, Powder Technol. 283 (2015) 254–259, https://doi.org/10.1016/j.powtec.2015.05.036.
[53] A.W. Weimer (Ed.), Carbide, Nitride and Boride Materials Synthesis and Processing, Springer Netherlands, Dordrecht, 1997, https://doi.org/10.1007/978-94-009-0071-4.
[54] H. Bel Fadhel, C. Frances, Wet batch grinding of alumina hydrate in a stirred bead mill, Powder Technol. 119 (2001) 257–268, https://doi.org/10.1016/S0032-5910(01)00266-2.
[55] T. Tanaka, Determining the optimum diameter of grinding media used for ultrafine grinding mechanisms, Adv. Powder Technol. 6 (1995) 125–137, https://doi.org/10.1163/156855295X00121.
[56] K. Ohenoja, M. Illikainen, J. Niinimäki, Effect of operational parameters and stress energies on the particle size distribution of TiO2 pigment in stirred media milling, Powder Technol. 234 (2013) 91–96, https://doi.org/10.1016/j.powtec.2012.09.038.
[57] M. Li, P. Alvarez, E. Bilgili, A microhydrodynamic rationale for selection of bead size in preparation of drug nanosuspensions via wet stirred media milling, Int. J. Pharm. 524 (2017) 178–192, https://doi.org/10.1016/j.ijpharm.2017.04.001.
[58] A. Strobel, J. Schwenger, S. Wittpahl, J. Schmidt, S. Romeis, W. Peukert, Assessing the influence of viscosity and milling bead size on the stressing conditions in a stirred media mill by single particle probes, Chem. Eng. Res. Des. 136 (2018) 859–869, https://doi.org/10.1016/j.cherd.2018.06.040.
[59] H. Gheisari, E. Karamian, M. Abdellahi, A novel hydroxyapatite –Hardystonite nanocomposite ceramic, Ceram. Int. 41 (2015) 5967–5975, https://doi.org/10.1016/j.ceramint.2015.01.033.
[60] A.M. Popa, J. Vleugels, J. Vermant, O. Van der Biest, Influence of surfactant addition sequence on the suspension properties and electrophoretic deposition behavior of alumina and zirconia, J. Eur. Ceram. Soc. 26 (2006) 933–939, https://doi.org/10.1016/j.jeurceramsoc.2004.12.023.
[61] M. Juhnke, D. Märtin, E. John, Generation of wear during the production of drug nanosuspensions by wet media milling, Eur. J. Pharm. Biopharm. 81 (2012) 214–222, https://doi.org/10.1016/j.ejpb.2012.01.005.
[62] H. Burrows, T. Chimamkpam, T. Encarnação, S. Fonseca, R. Pereira, M. Ramos, A. Valente, Trivalent metal ion binding to surfactants and polyelectrolytes : a review, J. Surf. Sci. Technol. 26 (2010) 197–212.
[63] R. Newburgh, J. Peidle, W. Rueckner, Einstein, Perrin, and the reality of atoms: 1905 revisited, American Journal of Physics - AMER J PHYS. 74 (2006), https://doi.org/10.1119/1.2188962.